J Membrane Biol (2010) 236:137–146
DOI 10.1007/s00232-010-9281-2

Magnetic Resonance Imaging Characteristics of Nonthermal Irreversible Electroporation in Vegetable Tissue

Mohammad Hjouj · Boris Rubinsky

Received: 23 December 2009 / Accepted: 22 June 2010 / Published online: 15 July 2010

Abstract We introduce and characterize the use of MRI for studying nonthermal irreversible electroporation (NTIRE) in a vegetative tissue model. NTIRE is a new minimally invasive surgical technique for tissue ablation in which microsecond, high electric-field pulses form nanoscale defects in the cell membrane that lead to cell death. Clinical NTIRE sequences were applied to a potato tuber tissue model. The potato is used for NTIRE studies because cell damage is readily visible with optical means through a natural oxidation process of released intracellular enzymes (polyphenol oxidase) and the formation of brown-black melanins. MRI sequences of the treated area were taken at various times before and after NTIRE and compared with photographic images. A comparison was made between T1W, T2W, FLAIR and STIR MRIs of NTIRE and photographic images. Some MRI sequences show changes in areas treated by irreversible electroporation. T1W and FLAIR produce brighter images of the treated areas. In contrast, the signal was lost from the treated area when a suppression technique, STIR, was used. There was similarity between optical photographic images of the treated tissue and MRIs of the same areas. This is the first study to characterize MRI of NTIRE in vegetative tissue. We find that NTIRE produces changes in vegetative tissue that can be imaged by certain MRI sequences. This could make MRI an effective tool to study the fundamentals of NTIRE in nonanimal tissue.

M. Hjouj (✉) · B. Rubinsky
Center for Bioengineering in the Service of Humanity and Society, School of Computer Science and Engineering, Hebrew University of Jerusalem, Jerusalem, Israel
e-mail: mhjouj@hotmail.com

Keywords Nonthermal irreversible electroporation · Cell membrane · MRI · T1-weighted · T2-weighted · FLAIR · STIR

Introduction

Electroporation, or electropermeabilization, is the biophysical phenomenon in which cell membrane permeability to ions and macromolecules is increased by exposing the cell to short (microsecond to millisecond) high electric-field pulses (EFPs) (Weaver 2000). The effect is related to the formation of defects (pores) in the cell membrane (Neumann et al. 1982). EFPs that induce electroporation in which defects reseal after the application of the pulse and the cells survive are known to cause "reversible electroporation." EFPs from which cells do not survive electroporation are known to cause "irreversible electroporation." Often, because of the electrical Joule heating phenomenon, irreversible electroporation EFPs also cause thermal damage to cells and tissues (Lee et al. 1988; Lee and Kolodney 1987). Nonthermal irreversible electroporation (NTIRE) refers to EFPs that induce irreversible electroporation without any thermal effects (Davalos et al. 2005). Other minimally invasive or noninvasive tissue ablation surgical techniques, such as radiation, cryosurgery, ultrasound, radiofrequency and microwave heating, affect indiscriminately all of the molecules in the volume of treated tissue. In contrast, NTIRE affects only the cell membrane lipid bilayer. This makes NTIRE unique among technologies for tissue ablation because it can ablate cells in a volume of tissue while leaving the extracellular matrix and other cell membrane components intact. Detailed information on NTIRE can be found in a recent edited book (Rubinsky 2010).

It has been recognized for decades (Gilbert et al. 1984) that intraoperative medical imaging monitoring is central to the successful use of minimally and noninvasive surgery. It is particularly valuable to have means to detect through medical imaging the successful application of the minimally invasive procedure. To this end, the outcome of NTIRE was examined with ultrasound (Lee et al. 2007; Onik et al. 2007; Rubinsky et al. 2007). Following NTIRE, ultrasound has shown a hypo-echoic image in the treated area, which turns within 24 h into a hyper-echoic one. The image was clearly visible in a vascular organ such as the liver (Lee et al. 2007; Rubinsky et al. 2007) but was not clear in avascular prostate tissue (Onik et al. 2007). This tentatively suggests that the image may be related to blood flow effects caused by the treatment and, thus, only an indirect measure of the NTIRE damage to cells.

We have undertaken this study to develop a tool for fundamental research on NTIRE as well as a first effort to develop a better understanding of the ability of magnetic resonance imaging (MRI) to image NTIRE-affected tissue. This first-order study was performed on potato vegetative tissue, which is a common medium for preliminary research in electroporation for several reasons. One of the reasons is that the effects of NTIRE on the cell membrane and the consequent MRI can be determined in vegetative tissue in the absence of blood flow, which otherwise may have an effect on the image. A more general reason is that following the replacement concept of the 3-Rs approach for animal testing (reduction of the number of animals, refinement of procedures to reduce distress and replacement of animal with nonanimal techniques, Russell and Burch 1959), it was recognized in the field of electroporation that some vegetables can be a proper alternative for studying bioelectrical aspects of tissue electroporation (Ivorra et al. 2009). In particular, raw potato tuber is a good choice because any irreversibly electroporated area will be distinctively darker about 5 h after electroporation, which can be seen by the naked eye and recorded by optical means. The browning reaction in the potato is one of the important areas of research in the food industry and was studied for well over half a century (e.g., Makover and Schwimmer 1954). It results from the oxidation of phenolic compounds under the action of an enzyme called polyphenoloxidase (PPO, phenolese). PPOs are a class of enzymes that were discovered in mushrooms and are widely distributed in nature. They appear to reside in the plastids and chloroplasts of plants. PPO is thought to play an important role in the resistance of plants to microbial and viral infections and to adverse climatic conditions. PPO also occurs in animals and is thought to increase disease resistance in insects and crustaceans. In the presence of oxygen from air, the enzyme catalyzes the first steps in the biochemical conversion of iron-containing phenolics that are also found in the potato to produce quinones, which undergo further polymerization to yield dark, insoluble polymers referred to as "melanins." Browning and the formation of melanins occur in the potato when the PPO enzyme is released through damaged cell membranes, such as in a cut or, in our case, irreversible electroporation. These melanins form barriers and have antimicrobial properties which prevent the spread of infection or bruising in plant tissues. A similar reaction occurs in crustaceans, e.g., shrimp, forming brown spots for the same purpose. The reaction leading eventually to the formation of melanin is very slow, and therefore, the photographic image of irreversible electroporation in the potato model takes hours to form. This long period of time until the browning occurs is indeed a major drawback of using the photographic or optical potato technique to study NTIRE and is one of the reasons for undertaking this study, in addition to developing a fundamental new method for studying NTIRE.

We designed this study in such a way as to explore various MRI sequences and to correlate MRIs with photographic images to develop a first-order understanding of NTIRE imaging with MRI. Our choice of the MRI sequences is based on the assumption that the primary effect is related to the damage to the cellular membrane and to the consequent release of intracellular content. We did not study the changes in water content that are observed in live tissue and are related to edema.

Materials and Methods

The study was performed on the Dutch-bred potato (*Solanum tuberosum* L. cv. Désirée), the world's most popular red-skinned, yellow-flesh main crop potato. All of the potatoes used in this study were from the same batch. To analyze the potato composition, fresh potatoes were homogenized and squeezed through a filtering pad (Padssan Gauze Pad, lot 3233), left for 10 min for precipitation of dissolved particles and filtered through a BD Falcon™ Cell Strainer, 40 μm nylon (352340; BD Bioscience, Bedford, MA). Potato homogenate was twice filtered through a 0.2-μm reverse-phase filter and subsequently analyzed using ion chromatography for nitrate, phosphate and sulfate content (ICS 300; Dionex, Sunnyvale, CA). Trace element analyses were performed by atomic emission spectroscopy (ICP ARCOS; Spectro, Kleve, Germany). For analysis, 2 ml of 65% nitric acid were added to 10 ml of potato filtrate and treated in a microwave,and a final volume of 25 ml was obtained by adding deionized water. The potato-treated filtrate composition is given in Table 1. Table 1 shows that this potato species is particularly rich in iron.

Table 1 Potato content analyses by ion chromatography and atomic emission spectroscopy

Substance	Concentration (mg/l)	Substance	Concentration (mg/l)
NO_3^-	1.4	Mn	2.08
PO_4^{-3}	975	Mo	0.087
SO_4^{-2}	77	Na	165
Ag	<0.0025	Ni	0.25
Al	4.7	P	563
As	<0.025	Pb	<0.025
B	1.37	S	363
Ba	0.043	Sb	<0.005
Ca	153	Se	<0.005
Cd	<0.0025	Si	12
Co	0.043	Sn	0.050
Cr	0.025	Sr	0.212
Cu	2.75	Ti	0.088
Fe	4.35	V	0.017
Hg	<0.003	Zn	5.25
K	4,900		
Li	0.09		
Mg	332		

Experiments were performed on 1-cm-thick slices of potatoes through which two 20-gauge stainless-steel needles were inserted parallel to each other at a distance of 1 cm between them, using a specially designed holder, which ensured the repeatability of the experiments. The experimental setup is shown in Fig. 1. For electroporation, the stainless-steel needles were connected to a conventional electroporator power supply (BTX 830; Harvard Apparatus, Holliston, MA). Preceding and following the electroporation, the potato was introduced into a Marconi Eclipse 1.5 T MRI scanner using a head coil, with the same sequences and acquisition parameters.

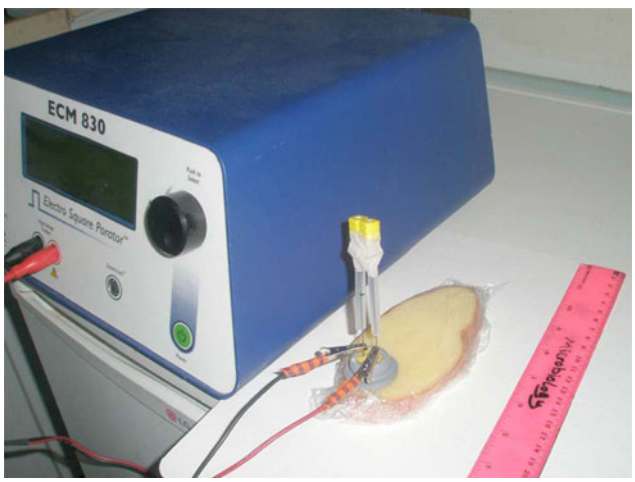

Fig. 1 Electroporation experimental setup showing the potato slice with the two electroporation needles inserted in it and the electroporation power supply

The primary goal of the study is determine whether MRI is an appropriate tool to monitor the effects of NTIRE on biological tissue. The study is based on application of NTIRE in a broad range of voltages that are typical of clinical electroporation (250–2,500 V) to a potato tuber as a biological tissue model. Various electroporation sequences were chosen according to the calculations in Davalos and Rubinsky (2008), to produce irreversible electroporation while avoiding thermal effects (NTIRE). The electroporation sequences are typical of those used in other IRE experiments (Lee et al. 2007; Onik et al. 2007; Rubinsky et al. 2007). Electroporation was followed by standard MRI techniques: spin-echo T1-weighted (SE T1W) and fast spin-echo T2-weighted (FSE T2W), SE short TI inversion recovery (STIR) and fluid attenuation inversion recovery (FLAIR). In addition, MRIs obtained at different times after the application of NTIRE were compared by conventional photography of the same samples.

Our original choice of the MRI sequences was based on the assumption that the primary effect is related to the damage to the cellular membrane and to the consequent release of intracellular content. It is anticipated that the main changes are therefore related to disruption of the cell membrane and a possible change in the signal from the phospholipids that form the cell membrane or from chemical changes due to the release of the intracellular contents—such as that related to the release of intracellular iron compounds and the eventual formation of melanin.

To this end, we chose sequences that assume that NTIRE caused cell membrane chemical composition-related relaxation effects, i.e., shortening of relaxation times T1 and T2. Therefore, we used conventional T1- and T2-weighted MRI, FLAIR sequences. To determine if the signal comes from phospholipids (lipid bilayer) or molecules with lipid like T1, we used a STIR sequence. STIR is used to eliminate signal from lipid or molecules with a T1 similar to that of lipid.

The MRI acquisition parameters used in this study were as follows: TE 19 ms, BW 10.4 kHz, TR 350 ms, NSA 3, matrix 192 × 256 for SE T1W images; TE 125 ms, BW 20.8 kHz, TR 3,500 ms, NSA 3, matrix 256 × 256, for FSE T2W images; TI 1800, TE 96 ms, BW 20.8, TR 8,000 ms, NSA 1, matrix 256 × 256 for FLAIR images; TI 150 ms, TE 10.5 ms, BW 25, TR 2,800 ms, NSA 2, matrix 192 × 256 for STIR images (for all sequences a 20-cm FOV, 3 mm slice thickness and no gap were used).

Photographs of MRI slices were taken using a digital camera (7.1 Mb; Olympus, Tokyo, Japan) for optical photography immediately after each MRI sequence. This was done to correlate between the area of oxidation (dark)

and the MRI in the same treated area at the same imaging period of time. Five repeats were done for every experimental condition in different potatoes.

Control experiments showed that insertion of the needles alone without EFPs does not produce any signal change in the treated area on MRIs.

Results

Results are presented as typical images from the experiments. Figures 2 and 3 are from the part of the study focusing on the MRI characteristics of irreversible electroporation. The electroporation protocol employed 25

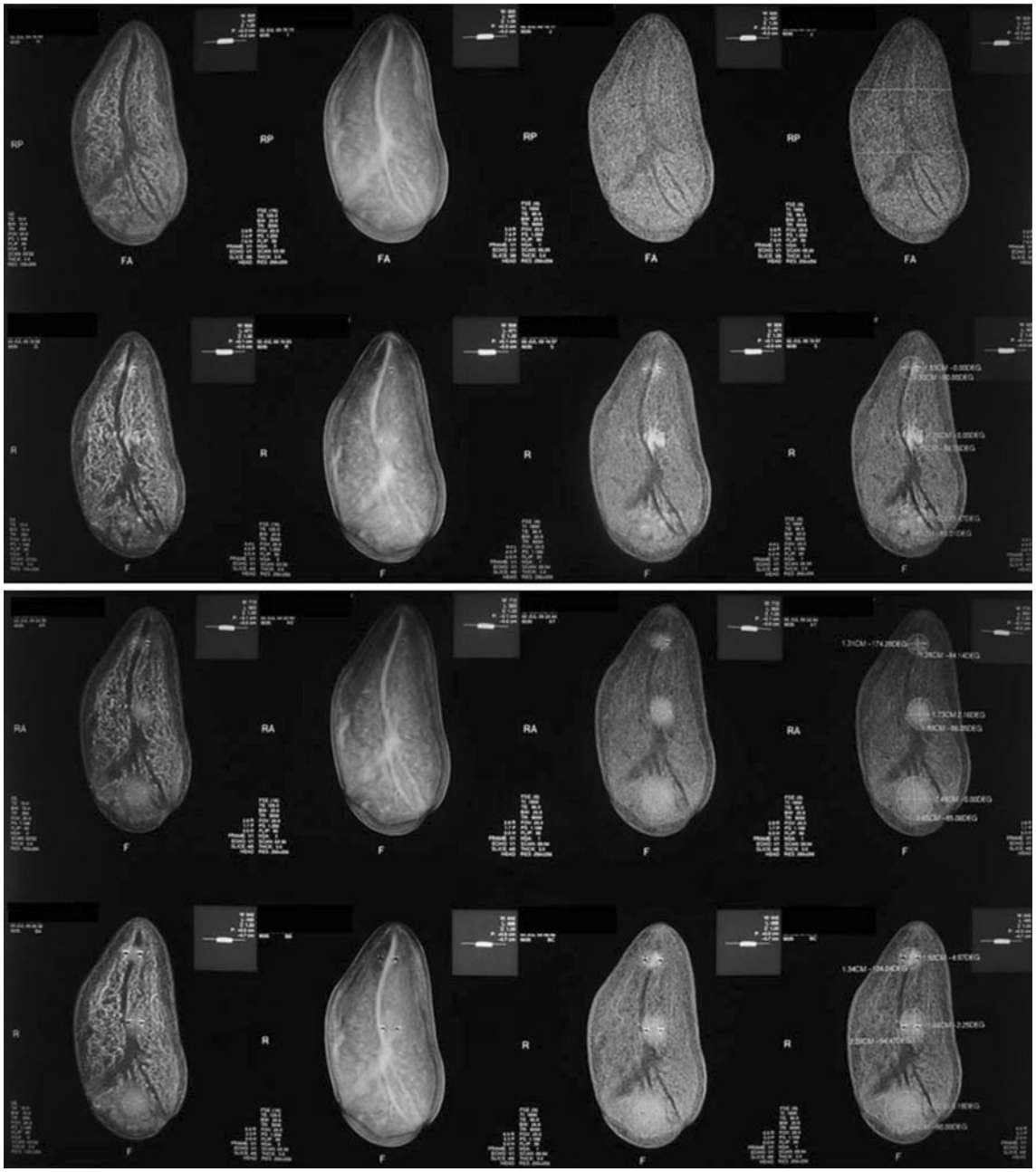

Fig. 2 Time-dependent MRIs of electroporated potato. *From left, first column* T1W images, *second column* T2W images, *third column* FLAIR images, *fourth column* FLAIR images with dimensions added on the figure. *From top, first row* untreated controls, *second row* 1 h after treatment, *third row* 6 h after treatment, *fourth row* 12 h after treatment. Treatment was done with a sequence of 25 100-μs pulses delivered at a frequency of 1 Hz. Three different voltages were applied during the treatment. In the top treated area of the potato the voltage between electrodes was 250 V, in the middle treated area of the potato the voltage between electrodes was 500 V and in the bottom treated area of the potato the voltage between the electrodes was 1,000 V. The *three round bright areas* seen best in the third and fourth columns are the treated areas

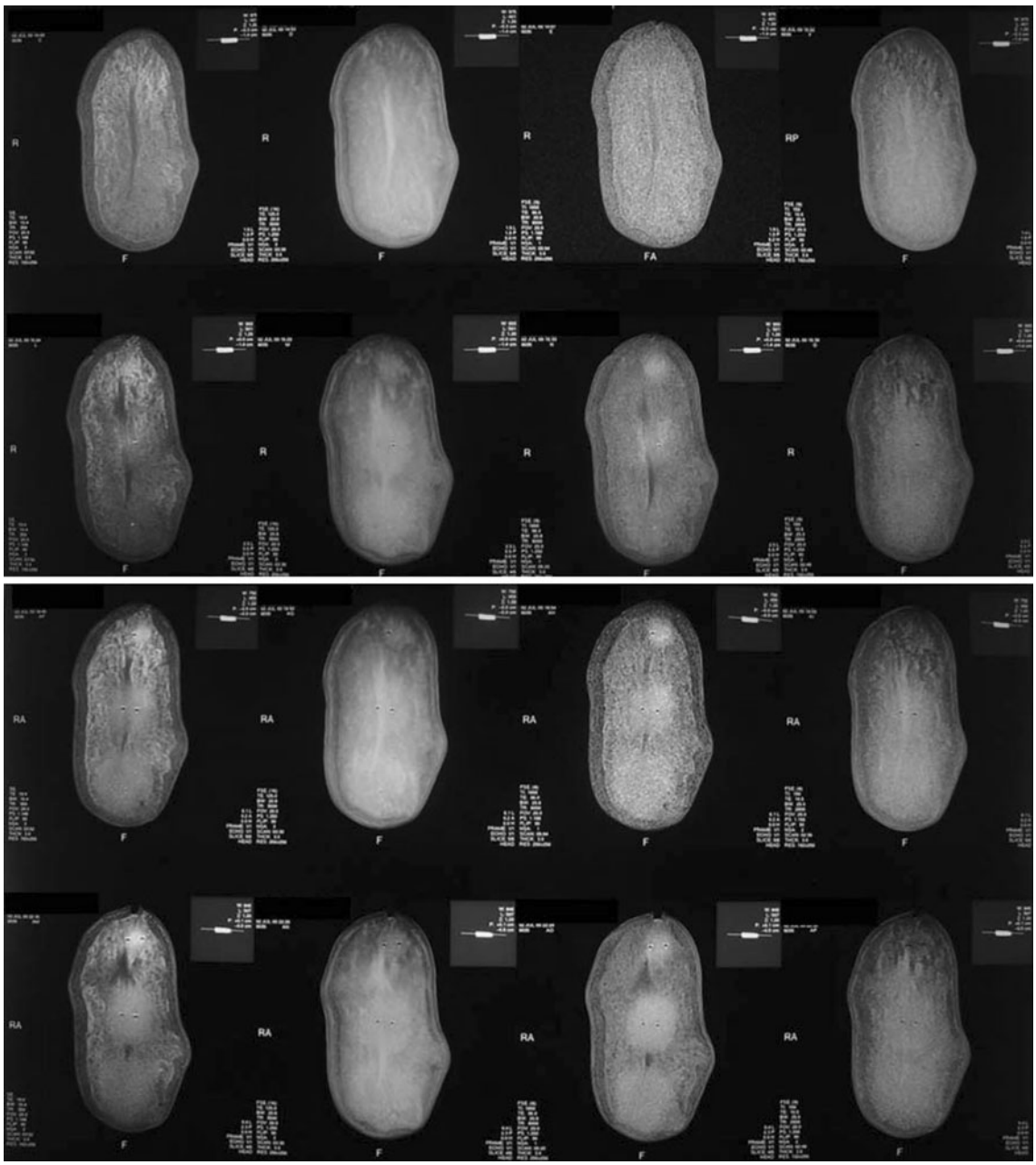

Fig. 3 Time-dependent MRIs of electroporated potato. *From left, first column* T1W images, *second column* T2W images, *third column* FLAIR images, *fourth column* STIR images. *From top, first row* untreated controls, *second row* 1 h after treatment, *third row* 6 h after treatment, *fourth row* 12 h after treatment. Treatment was done with a sequence of 25 100-μs pulses delivered at a frequency of 1 Hz. Three different voltages were applied during the treatment. In the top treated area of the potato the voltage between electrodes was 500 V, in the middle treated area of the potato the voltage between electrodes was 1,500 V and in the bottom treated area of the potato the voltage between the electrodes was 2,500 V. The *three round bright areas* seen in the third column (FLAIR) and lost in the fourth column (STIR) are the treated areas

pulses of 100 μs each delivered at a frequency of 1 Hz with the system shown in Fig. 1. The goal of this part of the study was to develop a first-order understanding of how irreversible electroporation affects MRIs and in the process to determine optimal MRI sequences for monitoring irreversible electroporation in the potato. Figures 2 and 3 are typical repeat experiments and show MRIs from two different electroporated potatoes as a function of time after application of the IRE pulses, for different MRI sequences and for different electrode voltages. The imaging sequences were T1W, T2W, FLAIR and STIR, as described in "Materials and Methods." Figure 2 was obtained for IRE with pulses of 250, 500 and 1,000 V applied on the electroporation electrodes. The electroporation treatment was

applied at three different locations on the potato, with the 250-V amplitude pulse at the top location, the 500-V amplitude pulse in the middle and the 1,000-V amplitude pulse at the bottom. Figure 3 was obtained for IRE with pulses of 500, 1,500 and 2,500 V applied on the electroporation electrodes. The IRE was applied at three different locations on the potato, with the 500-V amplitude pulse at the top location, the 1,500-V amplitude pulse in the middle and the 2,500-V amplitude pulse at the bottom. The figures compare the MRIs of untreated controls with MRIs of electroporated potatoes: 1, 3, 6 and 12 h after electroporation.

Figures 4 and 5 compare photographic images and FLAIR-MRI of irreversible electroporation-treated potatoes as a function of time after electroporation and for the various voltages applied to the electrodes. It is important to notice the regions of interest (ROI) in these figures, the volume of treated tissue where the electroporation was administered. Dark areas in the photographs are areas in which the cell enzymes have oxidized and are indicative of regions of cell membrane damage and release of intracellular content. Bright areas in the FLAIR-MRIs are the corresponding MRIs of the electroporation-treated area. Tables 2 and 3 show the evaluated dimensions of the areas that experienced electroporation-induced color change and MRI signal intensity changes in Figures 4 and 5, respectively.

Figure 6 is typical of a series of studies in which we observed the FLAIR-MRIs as a function of time from application of the NTIRE pulses. In these studies we noticed bright images as soon as the NTIRE-treated potatoes were introduced into the MRI, which increased with time and the applied voltage. Table 4 shows the evaluated typical dimensions of the bright areas on MRI.

Discussion

Certain MRI sequences can produce images of the NTIRE-treated areas which correspond to optical images showing color changes due to oxidation of the IRE-treated areas. The sequence dependence of the MRI of the NTIRE-treated area may shed some physical insight on the processes which occur during NTIRE.

In MRI, the tissue is investigated in a strong magnet equipped with three gradient coils, which allows shaping of the magnetic field in a controlled manner. The hydrogen protons are excited by radio frequency (RF) pulses. After the RF pulses, a process of spin relaxation occurs, which is controlled by factors like molecular motion (spin–lattice

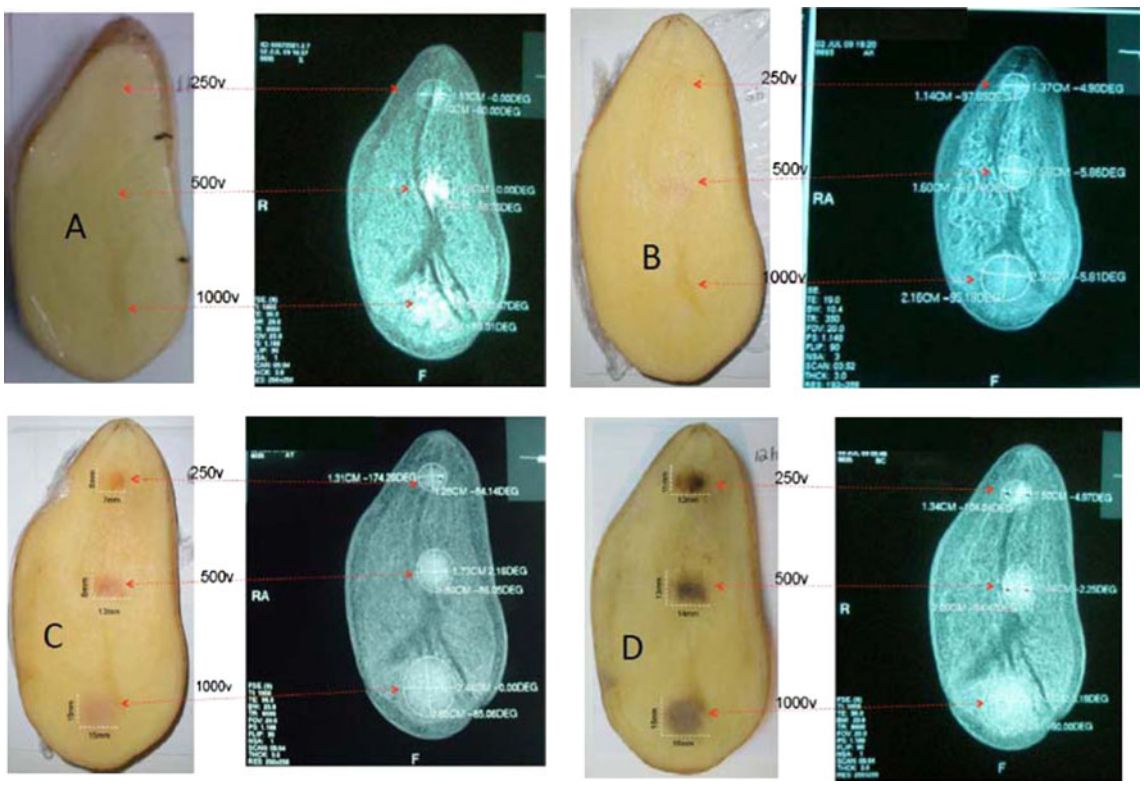

Fig. 4 Comparison between photographic images of the IRE-treated potato (*left*) and FLAIR-MRIs (*right*). The voltage used for electroporation is listed. The affected region is dark on the photographs due to oxidation and bright on the MRI due to the signals from the lipids. The dimensions of the affected areas are listed on the images. Times after IRE: **a** 1 h, **b** 3 h, **c** 6 h, **d** 12 h

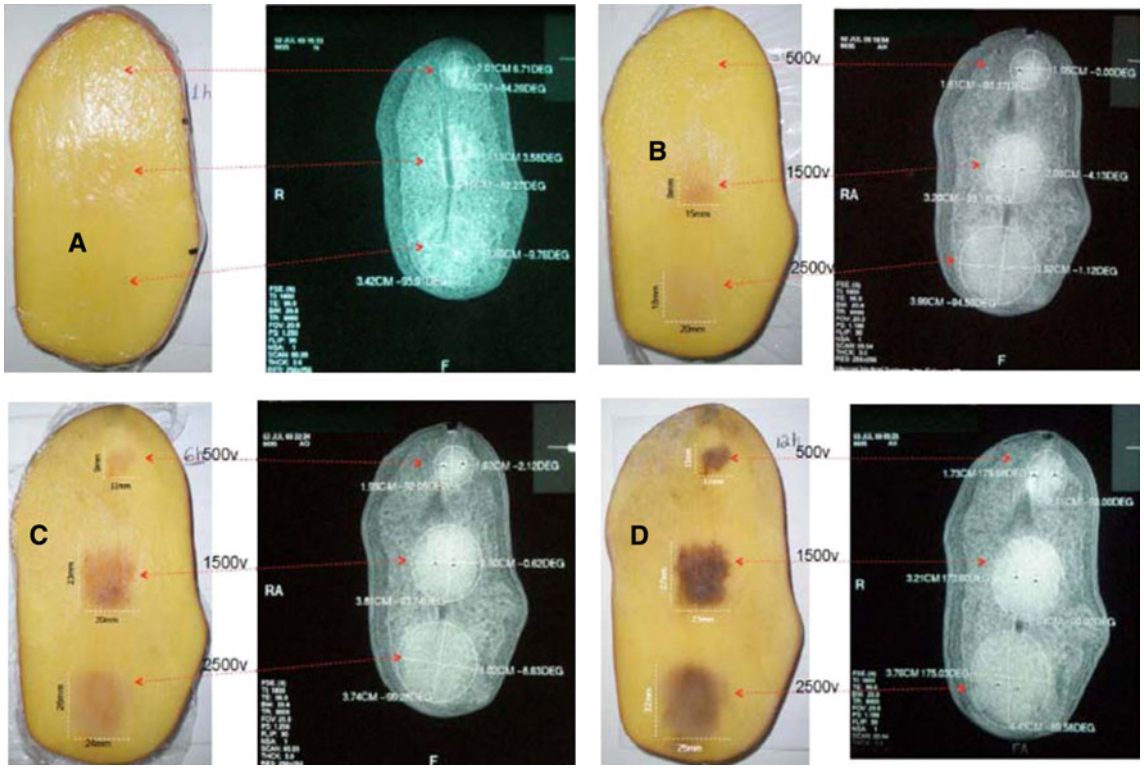

Fig. 5 Comparison between photographic images of the IRE-treated potato (*left*) and FLAIR-MRIs (*right*). The voltage used for electroporation is listed. The affected region is dark on the photographs due to oxidation and bright on the MRI due to the signals from the lipids. The dimensions of the affected areas are listed on the images. Times after IRE: **a** 1 h, **b** 3 h, **c** 6 h, **d** 12 h

Table 2 Diameters of the ROI on MRIs and oxidation zone in Fig. 4: diameters are length by width

Voltage	Oxidation zone on photograph (mm)	On MRI (mm)
1 h		
250 V upper	Not seen	11 × 13
500 V middle	Not seen	17 × 15
1,000 V lower	Not seen	21 × 20
3 h		
250 V upper	Not seen	11 × 13
500 V middle	Not seen	16 × 13
1,000 V lower	Not seen	21 × 20
6 h		
250 V upper	6 × 7	13 × 13
500 V middle	8 × 12	19 × 17
1,000 V lower	15 × 15	26 × 24
12 h		
250 V upper	11 × 12	14 × 13
500 V middle	13 × 14	19 × 18
1,000 V lower	16 × 16	30 × 26

interaction) that determines T1 characteristic relaxation times, dephasing due to interactions between molecules (spin–spin interactions) and main field inhomogeneities that determines T2 and T2* characteristic relaxation times. In this way, it is possible to image various characteristics of the proton distribution in the specimen.

The T1 characteristics of a tissue are determined by how far or close the natural motional frequencies of the protons of that tissue are to the Larmor frequency, which in turn is proportional to the magnetic field strength. Because of that, hydrogen protons in the small water molecule have higher natural motional frequencies than hydrogen protons in solid structure; hence, water has the longest T1 and lipids have the shortest T1. In a T1W image, the contrast is controlled by the T1 values of the tissue. Thus, it is possible to obtain images that reflect different physical properties.

T2 characteristics of a tissue are determined by how fast the dephasing of the spinning proton is in that tissue. For rapidly dephasing protons in solid-like tissue, T2 is short. In tissues where protons diphase slowly, like water, T2 is long. Thus, water has the strongest signal intensity in T2W images. Lipid tissue dephasing is less than in solids and more than in water. Therefore, T2 of lipid is intermediate and we expect intermediate signal intensity from lipid on our T2W images.

The inversion time (TI) value is used to affect the image contrast. The TR is chosen to be long (>4 × T1) so that it has little influence on contrast. This is what we have done in the FLAIR sequence (TI = 1,800 ms). TI is chosen to be

Table 3 Diameters of the ROI on MRIs and oxidation zone in Fig. 5: diameters are length by width

Voltage	Oxidation zone on photograph (mm)	On MRI (mm)
1 h		
500 V upper	Not seen	12 × 12
1,500 V middle	Not seen	21 × 19
2,500 V lower	Not seen	34 × 28
3 h		
500 V upper	Not seen	18 × 15
1,500 V middle	9 × 15	32 × 22
2,500 V lower	18 × 20	40 × 38
6 h		
500 V upper	9 × 11	17 × 16
1,500 V middle	23 × 20	35 × 28
2,500 V lower	26 × 24	37 × 34
12 h		
500 V upper	11 × 12	18 × 17
1,500 V middle	27 × 23	38 × 32
2,500 V lower	32 × 25	43 × 37

long enough so the tissue with the shorter T1 value provides the higher signal. In the STIR sequence we chose TI to be short (150 ms) where lipid or any tissue with T1 similar to lipid is at its null point and, thus, does not provide any signal.

The ROI are the locations in which the electroporation needles were inserted and the tissues around them affected by the EFPs, which appears brighter on MRI. The first column in Figs. 2 and 3 was obtained for T1W sequences. They show hyperintense signals (brighter) in the ROI almost immediately after electroporation. In a T1W image, the contrast is controlled by the T1 values of the tissue. Therefore, tissue with the shortest T1 will give the strongest signal. Since lipid has the shortest T1, the signal we start seeing after electroporation means that it may be from lipid or any other molecule with T1 similar to lipid. The signals in the ROI in the second column of Figs. 2 and 3 are not as clearly delineated as those in the first column, especially when the electroporation was done with lower voltages and at earlier times after the electroporation event. FLAIR images utilize a long inversion time in order to suppress the signal from fluid. After applying this sequence, we still see a strong (bright) signal in the ROI of the third column of images, which means that the tissue giving this strong signal has a T1 different from that of liquids. The STIR sequence is a special case of the inversion recovery–spin echo (IR-SE) pulse sequence. In this sequence TI is chosen to have such a value that the signal from lipid or any tissue with T1 similar to lipid is suppressed. The fourth column in Fig. 3 shows that the bright images from the ROI have disappeared. STIR suppresses the signal from lipid (or anything which has the same T1 as lipid). Because any bright image in the ROI is lost in STIR-MRI, the strong signals seen on T1 and FLAIR in the ROI are caused by lipid or a molecule with T1 similar to that of lipid.

This study reports that changes occur in the MRI signal of an electroporation-treated vegetable, the potato. The main value of this finding is that it suggests that MRI may be able to provide real-time imaging of electroporation events and could serve as a tool in studying NTIRE in potato tissue.

The explanation of the mechanism through which the MRIs were produced is tentative and requires more research. Tentatively, the observations made in this experimental study could be related to the mechanism of action of irreversible electroporation. The irreversible electroporation mode of cell death involves nanoscale defects in the cell membrane and a breach of the integrity of the cell membrane. One possible explanation for the observation in this study is that the lipids in the intact cell membrane are organized in a tight structure. Therefore, the protons in the molecule are not free to vibrate. When nanoscale molecular defects are induced in the cell membrane, the lipids in the membrane have additional degrees of freedom, resulting in a stronger signal in T1W images. This suggests that when irreversible electroporation is imaged with MRI a brighter image of the ROI is produced using imaging sequences that suppress the effects of the liquid and enhance the effects of lipids, such as the FLAIR sequence. The increase of signal with time may be related to further decomposition of the cell membrane. Obviously, this is only one possible explanation and much work remains to demonstrate the proposed mechanism.

Another explanation may be related to the high iron content of the potato, as shown in Table 1. The intracellular iron molecule is released by the breach in the cell membrane. The iron released in the ROI may shorten the T1 relaxation times of that region to be similar to that of lipids and, hence, respond in a similar way to the various sequences tested. Other chemical species that are released from the cell membrane and the intracellular content may have similar effects to lipids. For instance, melanin could be such a chemical species. However, an argument against melanin is that the MRIs of NTIRE formed in this study long before the slow-forming melanin and browning.

In summary, images obtained with FLAIR-MRI show the ROI to be much brighter. This sequence will be used in the presentation of the second part of the study. It should be mentioned that the experiments in the second part of the study were done with all of the imaging modalities. However, since the results with FLAIR were consistently much better, we will present the data only from this sequence in the interest of brevity.

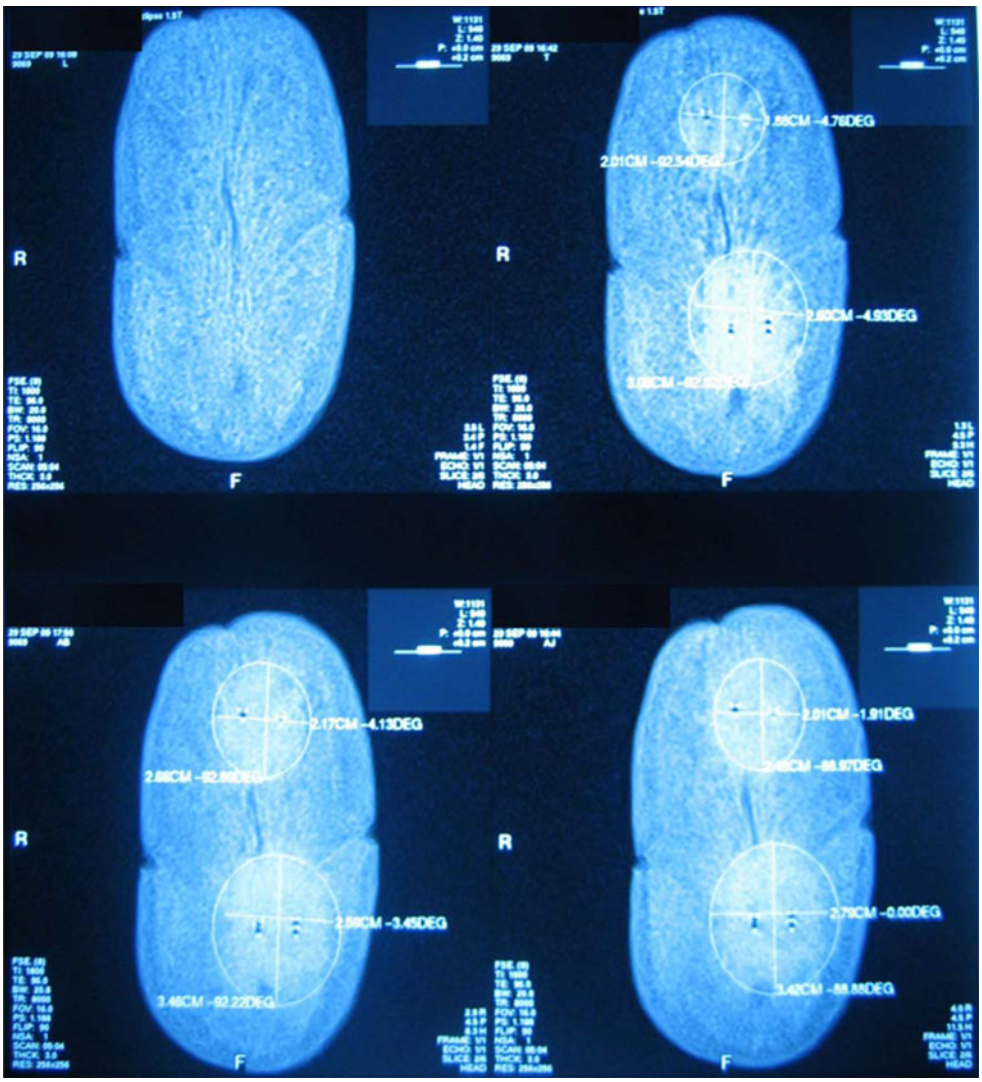

Fig. 6 Comparison between FLAIR-MRIs of the IRE-treated potato as a function of time after NTIRE treatment. *Clockwise from top left* Control, after 20 min, after 90 min and after 270 min. Pulses of 500 V form the top lesion and those of 2,500 V, the bottom lesion

Table 4 Diameters of the ROI on MRIs in Fig. 6: diameters are length by width

Voltage	ROI on MRI (mm)
20 min post-IRE	
500 V upper	20 × 18
2,500 V lower	30 × 26
90 min post-IRE	
500 V upper	26 × 21
2,500 V lower	34 × 25
270 min post-IRE	
500 V upper	26 × 21
2,500 V lower	34 × 27

Figures 4a and 5a show that 1 h after application of the IRE pulse, the optical images do not produce any evidence of cell membrane damage (the treated area has not darkened yet). In contrast, the MRIs already show an indication of substantial damage (bright areas), which seems to be larger the higher the pulse voltage. These figures suggest that the browning molecule, melanin, is by itself not related to the MRI sequence. In Figs. 4b and 5b, 3 h after application of the IRE pulses, the optical images still do not show any damage for voltages lower than 500 V. These observations address an important issue related to monitoring IRE. As with any other minimally invasive surgical procedure, it is important to monitor the extent of tissue damage. However, the mechanism of cell death in IRE is related to nanoscale defects of the cell membrane. In animal experiments (Edd et al. 2006), histology was unable to show cellular damage in the NTIRE-treated area until about 3 h after the NTIRE treatment was performed, when chemical reactions and the immune system began having an effect. It appears from this study that

FLAIR can detect the extent of cell death much earlier. This finding should be valuable in developing interventional protocols to monitor IRE in real time. Figures 4c, d and 5c, d demonstrate that the areas where the FLAIR-MRI signal has shown electroporation-induced changes were shown several hours later to have been indeed damaged through the enzyme oxidation color changes. However, the diagnostic MRI was made, in some cases, 5 h before the colorimetric enzyme oxidation test. Observing with optical means the sequence of tissue damage in time, it is also possible to observe that the extent of tissue ROI increases in time and that MRI predicts the actual extent of the area which will eventually oxidize and change color earlier, before oxidation occurs. It is possible that the cells at the periphery were partially damaged and that the process of necrosis takes time. This would be consistent with the observation that the larger the voltage applied on the electrodes, the larger is the damaged area. This is also consistent with mathematical models (e.g., Davalos et al. 2005; Davalos and Rubinsky 2008), which have shown that the electric field decreases from the electrode outward and that it increases at any location with an increase in the voltage applied to the electrodes. A higher electrical field results in a higher degree of irreversible electroporation, which is what the MRIs show. The ability of certain MRI sequences to detect cell death after minimally invasive surgery with irreversible electroporation may be of importance for monitoring this new minimally invasive surgical procedure.

In the studies that led to Fig. 6, we observed bright images in the treated area as soon as the treated potatoes were introduced into the MRI. At this stage we are still unable to perform NTIRE within the MRI and, therefore, we cannot know if the images are visible at the instant the electroporation is performed. This would be a very interesting topic of research, with fundamental as well as practical value.

In conclusion, a study on irreversible electroporation was performed using the potato as a model system. Several MRI sequences were tested to evaluate their ability to detect the effects of NTIRE as a function of time and electric pulses and in comparison with colorimetric enzyme oxidation tests. The study shows that MRI can produce an image of the irreversible electroporation-treated vegetative tissue. The study has shown that sequences weighted toward enhancing the T1 from lipid (or lipid-like molecules) and reducing that from liquid, such as FLAIR-MRI, provide better and much earlier indication of cell damage than the colorimetric tests. The mechanism is not clear. It may be related to the mechanism of cell damage by irreversible electroporation, which is related to disruption of the cell membrane lipid bilayer and formation of permanent nanoscale defects in the membrane, or it may be related to the release of intracellular molecules such as iron or other intracellular compounds. Regardless, MRI can become a valuable tool in studying NTIRE.

Acknowledgements This study was supported by a gift from the Adelson Family Foundation. We are grateful to the Medical Imaging Department, Makassed Hospital, Jerusalem, for making this study possible.

References

Davalos RV, Rubinsky B (2008) Temperature considerations during irreversible electroporation. Int J Heat Mass Transf 51: 5617–5622

Davalos RV, Mir IL, Rubinsky B (2005) Tissue ablation with irreversible electroporation. Ann Biomed Eng 33:223–231

Edd JF, Horowitz L, Davalos RV, Mir LM, Rubinsky B (2006) In vivo results of a new focal tissue ablation technique: irreversible electroporation. IEEE Trans Biomed Eng 53:1409–1415

Gilbert JC, Onik GM, Haddick W, Rubinsky B (1984) The use of ultrasonic imaging for monitoring cryosurgery. In: Proceedings of the 6th annual conference, IEEE engineering in medicine and biology, pp 107–112

Ivorra I, Mir LM, Rubinsky B (2009) Electric field redistribution due to conductivity changes during tissue electroporation: experiments with a simple vegetal model. In: World congress 2009 on medical physics and biomedical engineering, 7–12 Sept 2009, Munich, Germany, IFMBE proceedings, vol 25, pp 59–62

Lee RC, Kolodney MS (1987) Electrical injury mechanisms: electrical breakdown of cell membranes. Plast Reconstr Surg 80:672–679

Lee RC, Gaylor DC, Bhatt D, Israel DA (1988) Role of cell membrane rupture in the pathogenesis of electrical trauma. J Surg Res 44:709–719

Lee EW, Loh CT, Kee ST (2007) Imaging guided percutaneous irreversible electroporation: ultrasound and immunohistological correlation. Technol Cancer Res Treat 6:287–294

Makover RU, Schwimmer S (1954) Inhibition of enzymic color formation in potato by ATP. Biochim Biophys Acta 14:156–157

Neumann E, Schaefer-Ridder M, Wang Y, Hofschneider PH (1982) Gene transfer into mouse lyoma cells by electroporation in high electric fields. EMBO J 1:841–845

Onik G, Mikus P, Rubinsky B (2007) Irreversible electroporation: implications for prostate ablation. Technol Cancer Res Treat 6:295–300

Rubinsky B (ed) (2010) Irreversible electroporation. Series in Biomedical Engineering XIV. Springer, New York

Rubinsky B, Onik G, Mikus P (2007) Irreversible electroporation: a new ablation modality—clinical implications. Technol Cancer Res Treat 6:37–48

Russell WMS, Burch RL (1959) The principles of humane experimental technique. Methuen, London

Weaver JC (2000) Electroporation of cells and tissues. IEEE Trans Plasma Sci 28:24–33